JOURNAL OF SOLID STATE CHEMISTRY **126,** 80–87 (1996)
ARTICLE NO. 0313

Thermodynamic Investigation on the BaB_2O_4–BaF_2–2NaF–$Na_2B_2O_4$ Reciprocal System

Weidong Zhuang and Guanghui Rao

Institute of Physics, Chinese Academy of Sciences, P.O. Box 603, Beijing 100080, People's Republic of China

Jingkui Liang

Institute of Physics, Chinese Academy of Sciences, P.O. Box 603, Beijing 100080, People's Republic of China; and International Centre for Materials Physics, Chinese Academy of Sciences, Shenyang 110015, People's Republic of China

Yuling Zhang and Ying Shi

Institute of Physics, Chinese Academy of Sciences, P.O. Box 603, Beijing 100080, People's Republic of China

Zhiyu Qiao

Department of Physical Chemistry, University of Science and Technology Beijing, Beijing 100083, People's Republic of China

and

Jianyun Shen

General Research Institute for Non-ferrous Metals, Beijing 100088, People's Republic of China

Received February 6, 1996; accepted June 20, 1996

The BaB_2O_4–BaF_2–2NaF–NaB_2O_4 reciprocal system has been investigated by combination of experimental measurements with theoretical calculation. The $Na_2B_2O_4$–2NaF binary and $Na_2B_2O_4$–BaF_2 pseudo-binary phase diagrams are measured by means of DTA and X-ray diffraction. The thermodynamic functions for all sub-binary systems are derived from measured phase diagrams and thermodynamic data by CALPHAD technique, and the sub-binary phase diagrams are calculated according to phase equilibrium principle. Then, the thermodynamic functions for sub-binary systems are extrapolated to the BaB_2O_4–BaF_2–2NaF–$Na_2B_2O_4$ reciprocal system, and the phase diagram of the reciprocal system is calculated. The calculated phase diagrams are verified by additional experiments.

1. INTRODUCTION

Many metaborates have potential nonlinear optical properties. The low-temperature form of barium metaborate (β-BaB_2O_4) is an excellent ultraviolet SHG (Second Harmonic Generator) material (1). It has high efficiency, excellent homogeneous optic properties, high damage threshold value, and low production cost.

BaB_2O_4 has two polymorphisms (2), a high-temperature form (α-BaB_2O_4) and a low-temperature form (β-BaB_2O_4), with a polymorphic transition at 920 ± 10°C (3). The melting point of α-BaB_2O_4 is 1095 ± 5°C (4). The single crystal of α-BaB_2O_4 could be grown directly from melt by the Czochralski method, but it has no second harmonic effect. Although β-BaB_2O_4, having a second harmonic effect, could be obtained by annealing α-BaB_2O_4 at low temperature, the resultant crystal would crack seriously due to polymorphic transition, and is not suitable for investigation (4). In order to choose a proper flux, which will lower the eutectic temperature and increase the temperature and composition range for growth of β-BaB_2O_4, to improve the growth condition of β-BaB_2O_4, and to obtain a large-size perfect β-BaB_2O_4 single crystal, a great deal of study on phase relations in the systems containing BaB_2O_4 has been carried out in our group (4–13).

The development of the CALPHAD (CALculation of PHAse Diagram) technique, the essence of which is the computer coupling of phase diagrams and thermodynamics, helps us a great deal in unifying the theoretical investigation, experimental measurement, and geometrical description of phase diagrams and thermodynamics. In this technique, all available phase diagram and thermodynamic

0022-4596/96 $18.00

data for a system are simultaneously evaluated in order to obtain a set of equations describing the thermodynamic properties of the phases as functions of temperature and composition. In this way, the phase diagram and thermodynamic data can be critically assessed in a therodynamically self-consistent manner. The phase diagram can subsequently be calculated by computer from the thermodynamic equations. Hence, all the thermodynamic properties as well as the phase diagram can usually be represented and stored by means of a small set of coefficients. Furthermore, the self-consistent analytical representation permits the data to be interpolated and extrapolated. The procedure greatly reduces the amount of data needed to characterize fully a binary system.

Of particular importance of the CALPHAD technique is the fact that it is often possible to estimate the thermodynamic properties and phase diagrams of ternary and higher-order systems from assessed parameters for their sub-binary systems. If measured ternary data are available for a system, these can be used to refine the representation of the ternary thermodynamic properties. This technique has been applied to a large number of alloy and ionic salt systems (14–17).

In this work, the BaB_2O_4–BaF_2–2NaF–$Na_2B_2O_4$ reciprocal system was investigated by DTA (Differential Thermal Analysis) and XRD (X-ray diffraction) measurements as well as by the CALPHAD technique. First, the $Na_2B_2O_4$–2NaF binary and the $Na_2B_2O_4$–BaF_2 pseudo-binary phase diagrams were measured by DTA and XRD methods. Then, the thermodynamic functions for four sub-binary systems and the $Na_2B_2O_4$–BaF_2 pseudo-binary system were derived from measured phase diagrams and thermodynamic data by the CALPHAD technique. The sub-binary and pseudo-binary phase diagrams were calculated thereafter according to the phase equilibrium principle. After that, the thermodynamic functions for sub-binary systems were extrapolated to the BaB_2O_4–BaF_2–2NaF–$Na_2B_2O_4$ reciprocal system, and the phase diagram of the reciprocal system was calculated. To verify the reliability of the calculated phase diagram, additional experiments were made and compared with the calculated results.

2. EXPERIMENTAL PROCEDURE

2.1. Sample Preparation

To synthesize pure BaB_2O_4 and $Na_2B_2O_4$, analytical agents $BaCO_3$ and Na_2CO_3 were respectively mixed with H_3BO_3 in a molar ratio of 1:2 with a proper excess of H_3BO_3. The mixtures were sintered at 1000–1200°C for 4 h, then crystallized at about 700°C for 10 h before cooling to room temperature. The synthesized products melted congruently in DTA experiments, and were confirmed to be the expected components by X-ray diffraction.

The sample were prepared by mixing the synthesized BaB_2O_4, $Na_2B_2O_4$, and analytical agents NaF and BaF_2 in the expected molar ratio. The mixtures were melted and then cooled to appropriate temperature for crystallization. To check the homogeneity of the prepared sample, powders of some samples were annealed at 400–600°C for 10 days. Both DTA and XRD showed no difference between annealed and unannealed samples. This means that the prepared samples were well homogeneous.

2.2. Measurement

Phase analysis of the samples was carried out by X-ray diffraction. A Guinier–de Wolff monochromatic focusing camera and Co$K\alpha$ or Cu$K\alpha$ radiation were used. Pure Si powder was added to specimens as an inner standard.

Differential thermal analysis was performed with a homemade CR-G type high-temperature DTA apparatus. α-Al_2O_3 powder and Pt crucible were used as reference material and container, respectively. Pt–PtRh thermocouples were used for control and measurement of temperature. The powder specimen was made to contact the Pt crucible as closely as possible in order to get a good baseline. The heating rate was 10°C/min. The extrapolated onset temperature of differential thermal peak in heating curve was taken as the phase transition and liquidus temperature. The accuracy of the measured temperature, which was calibrated by the melting point of Au (1063°C) and phase transition temperature of SiO_2 (573°C), was ±3°C.

3. EXPERIMENTAL RESULTS

3.1. $Na_2B_2O_4$–2NaF System

Compositions of samples and DTA results obtained on heating curves are plotted in the calculated $Na_2B_2O_4$–2NaF

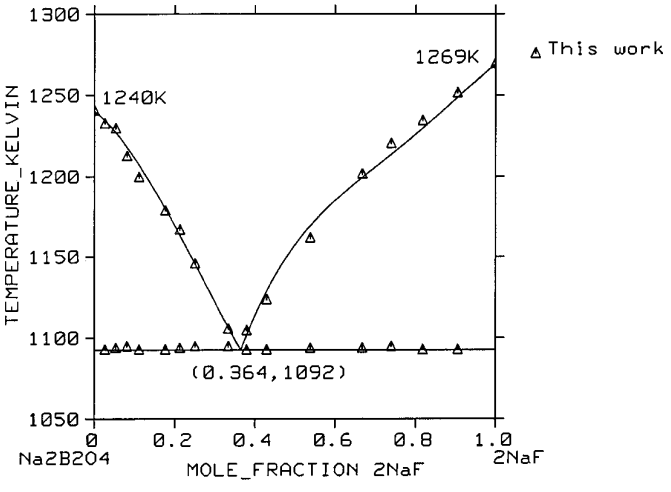

FIG. 1. Phase diagram of the $Na_2B_2O_4$–2NaF binary system.

TABLE 1
Compositions and Results of XRD Phase Analysis of the Samples in the $Na_2B_2O_4$–BaF_2 Pseudo-binary System

No.	x_{BaF_2}	Phases	No.	x_{BaF_2}	Phases
1	0.00	$Na_2B_2O_4$	10	0.60	B, BaF_2
2	0.05	$Na_2B_2O_4$, B[a]	11	0.65	B, BaF_2
3	0.10	$Na_2B_2O_4$, B	12	0.70	B, BaF_2
4	0.15	$Na_2B_2O_4$, B	13	0.75	B, BaF_2
5	0.20	$Na_2B_2O_4$, B	14	0.80	B, BaF_2
6	0.25	$Na_2B_2O_4$, B	15	0.85	B, BaF_2
7	0.30	$Na_2B_2O_4$, B	16	0.90	B, BaF_2
8	0.40	B	17	0.95	B, BaF_2
9	0.50	B, BaF_2	18	1.00	BaF_2

[a] B represents $0.6Na_2B_2O_4 \cdot 0.4BaF_2$.

phase diagram in Fig. 1. No solid solubility or intermediate compounds have been observed from the X-ray powder diffraction patterns of the samples. The measured eutectic point is located at $T = 820 \pm 3$°C, $X_{2NaF} = 0.36 \pm 0.01$.

3.2. $Na_2B_2O_4$–BaF_2 System

Compositions and the results of XRD phase analysis of the samples are listed in Table 1. The results of XRD phase analysis show that $Na_2B_2O_4$–BaF_2 is the stable diagonal in the BaB_2O_4–BaF_2–2NaF–Na_2O_4 reciprocal system. The results of XRD phase analysis also show that a new compound was synthesised with the composition $X_{BaF_2} = 0.4$. We name this new compound $0.6Na_2B_2O_4 \cdot 0.4BaF_2$. This compound melts congruently at 775 ± 3°c. DTA results obtained on heating curves are plotted in the calculated $Na_2B_2O_4$–BaF_2 phase diagram in Fig. 2. The measured eutectic point of $Na_2B_2O_4$ and $0.6Na_2B_2O_4 \cdot 0.4BaF_2$ is located at $T = 751 \pm 3$°C, $X_{BaF_2} = 0.35 \pm 0.01$, and the measured eutectic point of $0.6Na_2B_2O_4 \cdot 0.4BaF_2$ and BaF_2 is located at $T = 629 \pm 3$°C, $X_{BaF_2} = 0.67 \pm 0.01$.

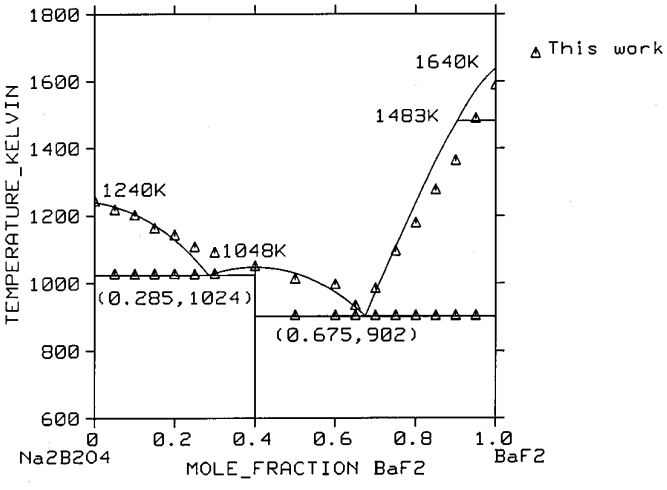

FIG. 2. Phase diagram of the $Na_2B_2O_4$–BaF_2 pseudo-binary system.

4. OPTIMIZATION AND CALCULATION

4.1. Information of Phase Diagrams and Thermodynamic Data

Thermodynamic data of component compounds. Knacke *et al.* (18) compiled the thermodynamic data of $Na_2B_2O_4$, BaF_2, and NaF. BaF_2 has two polymorphisms, a low-temperature form (α- BaF_2) and a high-temperature form (β-BaF_2), with a polymorphic transition at 1480 K. No experimental thermodynamic data of BaB_2O_4 have been reported. Chen (19) optimized the Gibbs energy of formation of α-BaB_2O_4 and β-BaB_2O_4; these data were used in the subsequent optimization and calculation. Compared with the heat of fusion of BaB_4O_7 (20), BaB_8O_{13} (20), CaB_2O_4 (18), and $Na_2B_2O_4$ (18), the heat of fusion of BaB_2O_4 optimized by Chen (19) may be too small. In our early work (9), the heat of fusion of α-BaB_2O_4 was estimated from the experimental phase diagrams according to the equation (21)

$$\lim_{x_i \to 1} \left(\frac{dx_i^l}{dT} - \frac{dx_i^s}{dT} \right) = \frac{\Delta^\circ H_{f(i)}}{\nu R T_{f(i)}^2}. \quad [1]$$

In this work, the estimated data (9) was taken instead of the data optimized by Chen (19).

All the thermodynamic data of component compounds were transformed to the temperature dependence of Gibbs energy (Section 4.2 and Table 2).

BaB_2O_4–$Na_2B_2O_4$ system. We have measured the BaB_2O_4–$Na_2B_2O_4$ phase diagram (4) early by means of DTA and XRD methods. This system is a simple eutectic one with the eutectic point at $T = 826 + 5$°C, $X_{Na_2B_2O_4} = 0.5$.

BaB_2O_4–BaF_2 system. The BaB_2O_4–BaF_2 phase diagram was reported in Ref. (12). The results of DTA and XRD measurements show that a new compound, $BaBO_2F$, was synthesized. This compound melts congruently at 867 ± 3°C. The eutectic points of $BaBO_2F$ with BaB_2O_4 and BaF_2 are located at $T = 749 \pm 3$°C, $X_{BaF_2} = 0.40$ and $T = 815 \pm 3$°C, $X_{BaF_2} = 0.57$, respectively.

2NaF–BaF_2 system. In the 2NaF–BaF_2 phase diagram measured by Bergman and Banashek (22) in 1953, the eutectic point is at $T = 812$°C, $X_{BaF_2} = 0.54$. The eutectic point is located at $T = 825$°C, $X_{BaF_2} = 0.53$ in the 2NaF–BaF_2 phase diagram measured by Grube (23) in 1927. Bukhalova and Yajub'yan (28) were interested in measurement of melt densities and derived the 2NaF–BaF_2 phase diagram from Ref. (22). The results of Bergman and Banashek (22) were used in our optimization. Hong and Kleppa (24) measured the mixing enthalpies of liquid at 1354 K

TABLE 2
Gibbs Energy of all Phases of Component Compounds (J/mol) ($^\circ G_i^\phi(T) = a + bT + cT\ln T + dT^2 + e/T + fT^3$, T in K)

Phase	a	b	c	d	e	f	Range
α-BaB_2O_4	−2002773.64	586.068	−107.587	−0.040014	964499.9	0	298–2000 K
β-BaB_2O_4	−2006352.64	589.068	−107.587	−0.040014	964499.9	0	298–2000 K
BaB_2O_4 (liquid)	−1934989.64	536.518	−107.587	−0.040014	964499.9	0	298–2000 K
α-BaF_2	−1221465.00	110.841	−29.029	−0.038476	−903499.9	0	298–1310 K
	−1273562.00	739.358	−118.148	0	0	0	1310–2000 K
β-BaF_2	−1255358.00	650.457	−107.654	0	0	0	298–2000 K
BaF_2 (liquid)	−1218082.00	564.856	−99.161	0	0	0	298–2000 K
2NaF (solid)	−1177324.00	513.334	−90.098	−0.016041	259000.0	0	298–2000 K
2NaF (liquid)	−1146570.00	821.890	−139.494	0	0	0	298–2000 K
$Na_2B_2O_4$ (solid)	−2013289.00	953.155	−159.076	−0.023556	1841000.0	0	298–2000 K
$Na_2B_2O_4$ (liquid)	−2068890.00	1923.052	−292.880	0	0	0	298–2000 K

Note. Reference states are the pure solid elements in their stable states at 298.15 K.

in this system by means of the calorimetric method. The mixing enthalpies are small and less than 1 kJ/mol.

4.2. Thermodynamic Model

Reference state. As reference states for this reciprocal system, the pure solid elements in their stable states at 298.15 K (Stable Element Reference, SER) were chosen. The temperature dependence of the Gibbs energy of the component compounds is given in the form

$$^\circ G_i^\phi(T) = a + bT + cT\ln T + dT^2 + e/T + fT^3, \quad [2]$$

where $^\circ G_i^\phi(T)$ is the molar Gibbs energy of phase ϕ of compound i at temperature T(K). In different temperature ranges different sets of the coefficients a to f may be used. The values of the coefficients are listed in Table 2.

Intermediate phases. Intermediate phases, $BaBO_2F$(A) and $0.6Na_2B_2O_4 \cdot 0.4BaF_2$(B), were modeled as stoichiometric phases. The Gibbs energy for solid $BaBO_2F$ and $0.6Na_2B_2O_4 \cdot 0.4BaF_2$ were given by the formulas

$$^\circ G_A^s(T) = 0.5{}^\circ G^\beta_{BaB_2O_4}(T) + 0.5{}^\circ G^\alpha_{BaF_2}(T) + a_A + b_A T \quad [3]$$

and

$$^\circ G_B^s(T) = 0.6{}^\circ G^s_{Na_2B_2O_4}(T) + 0.4{}^\circ G^\alpha_{BaF_2}(T) + a_B + b_B T, \quad [4]$$

respectively.

Liquid phase. The Gibbs energy of the liquid phase can be divided into three parts, the reference part (ref), the ideal mixing part (id), and the excess part (E):

$$G^l = {}^{ref}G^l + {}^{id}G^l + {}^{E}G^l. \quad [5]$$

For binary system 1–2,

$${}^{ref}G^l = x_1{}^\circ G_1^l + x_2{}^\circ G_2^l \quad [6]$$

$${}^{id}G^l = RT(x_1\ln x_1 + x_2\ln x_2). \quad [7]$$

The excess term is the function of the concentration represented by the Redlich–Kister polynomial (25)

$${}^{E}G^l = x_1x_2L_{12} = x_1x_2\sum_{i=0}^{n}(a_i + b_iT)(x_1 - x_2)^i. \quad [8]$$

For the C,D/X,Y reciprocal system (BaB_2O_4–BaF_2–2NaF–$Na_2B_2O_4$ reciprocal system can be written as Ba^{2+}, $2Na^+/B_2O_4^{2-}$, $2F^-$),

TABLE 3
The Optimized Parameters of Liquid Phase in the BaB_2O_4–BaF_2–2NaF–$Na_2B_2O_4$ Reciprocal System (J/mol)

System	i	a_i	b_i
BaB_2O_4–$Na_2B_2O_4$	0	−16564.68	0
	1	−12318.47	0
BaB_2O_4–BaF_2	0	−99615.44	0
	1	−30015.81	0
$Na_2B_2O_4$–2NaF	0	−6783.14	0
	1	−10014.21	0
	2	−6587.47	0
2NaF–BaF_2	0	−2516.04	−11.051
	1	2297.47	4.069
$Na_2B_2O_4$–BaF_2	0	−105019.04	0
	1	3990.53	0

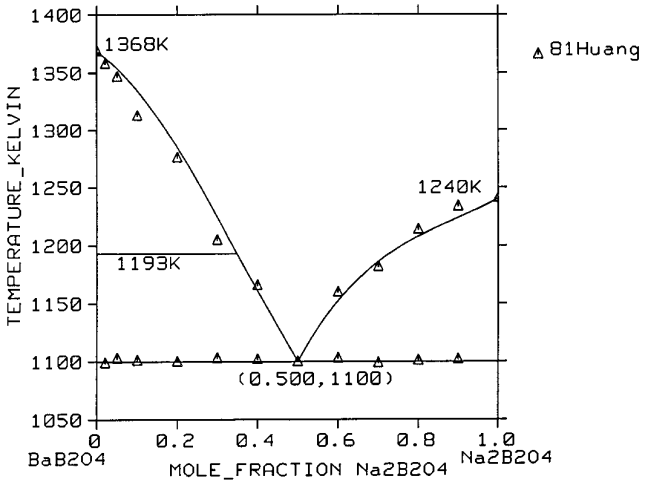

FIG. 3. Phase diagram of the BaB_2O_4–$Na_2B_2O_4$ binary system.

$$^{ref}G^{l} = x_C x_X {}^{\circ}G^{l}_{CX} + x_D x_X {}^{\circ}G^{l}_{DX} + x_C x_Y {}^{\circ}G^{l}_{CY} + x_D x_Y {}^{\circ}G^{l}_{DY} \quad [9]$$

$$^{id}G^{l} = RT(x_C \ln x_C + x_D \ln x_D + x_X \ln x_X + x_Y \ln x_Y) \quad [10]$$

$$^{E}G^{l} = x_C x_D x_X L_{C,D:X} + x_C x_D x_Y L_{C,D:Y} + x_C x_X x_Y L_{C:X,Y} + x_D x_X x_Y L_{D:X,Y} + x_C x_D x_X x_Y L_{C,D:X,Y}, \quad [11]$$

where $x_C + x_D = 1$, $x_X + x_Y = 1$; ${}^{\circ}G^{l}_{CX}$, ${}^{\circ}G^{l}_{DX}$, ${}^{\circ}G^{l}_{CY}$, and ${}^{\circ}G^{l}_{DY}$ are the Gibbs energies of liquid for the four component compounds; $L_{C,D:X}$, $L_{C,D:Y}$, $L_{C:X,Y}$, and $L_{D:X,Y}$ are the parameters for four sub-binary systems; $L_{C,D:X,Y}$ is the "reciprocal" parameter. In the $Ba^{2+}, 2Na^{+}/B_2O_4^{2-}, 2F^{-}$ reciprocal system, $Na_2B_2O_4$–BaF_2 is the stable diagonal; the optimized parameter of the $Na_2B_2O_4$–BaF_2 pseudo-binary system is taken as the "reciprocal" parameter in this work.

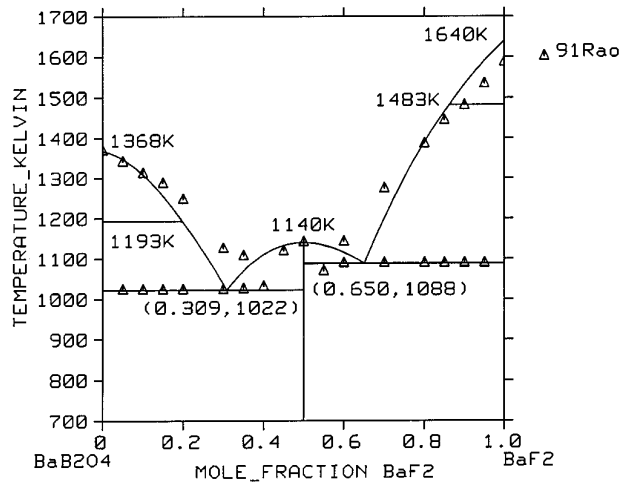

FIG. 4. Phase diagram of the BaB_2O_4–BaF_2 binary system.

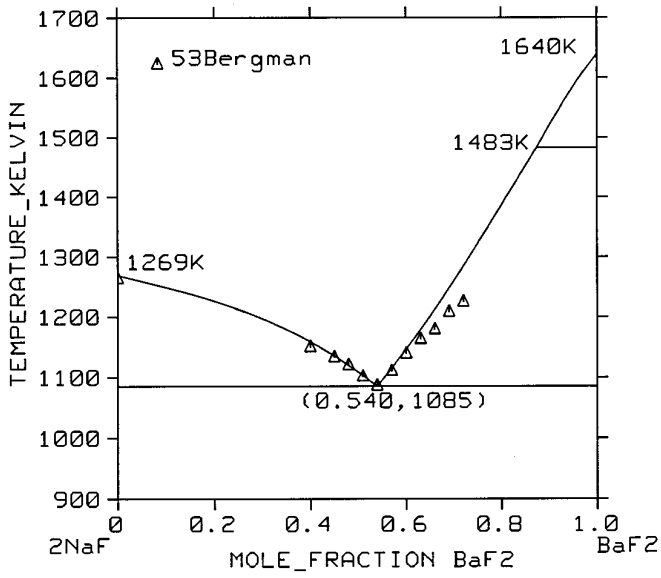

FIG. 5. Phase diagram of the $2NaF$–BaF_2 binary system.

4.3. Optimization of Binary Systems

BaB_2O_4–$Na_2B_2O_4$ system. The optimized parameters of the liquid phase derived from the measured phase diagram (4) with $i = 1$ in Eq. [8] are listed in Table 3. The calculated phase diagram is shown in Fig. 3. The calculated eutectic point is at $T = 1100$ K, $X_{Na_2B_2O_4} = 0.500$, which is in agreement with the measured value in Ref. (4).

BaB_2O_4–BaF_2 system. The optimized parameters of

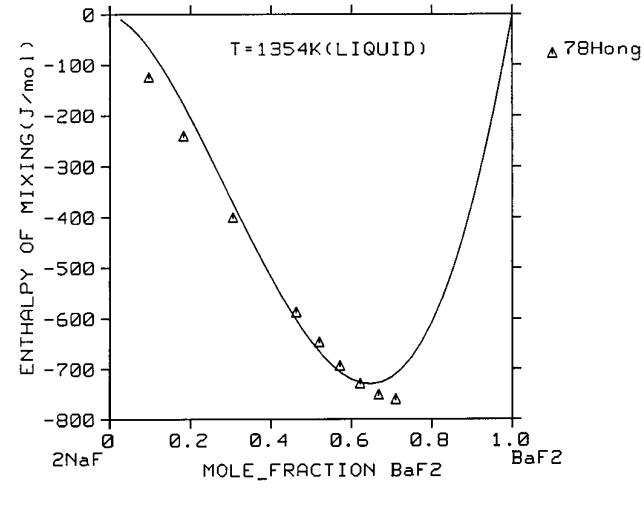

FIG. 6. Calculated mixing enthalpy of the liquid phase with measured data (24) for the $2NaF$–BaF_2 binary system at 1354 K.

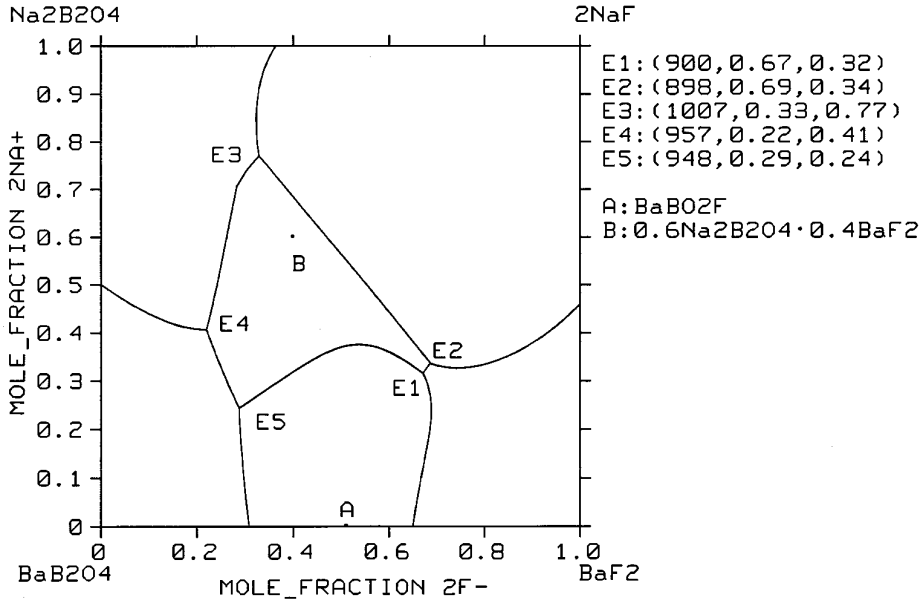

FIG. 7. Calculated liquid projection of the BaB_2O_4–BaF_2–2NaF–$Na_2B_2O_4$ reciprocal system (temperatures of eutectic points E1 to E5 in K).

the liquid phase derived from the measured phase diagram (12) with $i = 1$ in Eq. [8] are listed in Table 3. The Gibbs energy for solid $BaBO_2F$ was also optimized with $a_A = -21244.91$J/mol, $b_B = 0$ in Eq. [3]. The calculated phase diagram is shown in Fig. 4. The calculated eutectic points are at $T = 1022$ K, $X_{BaF_2} = 0.309$ and $T = 1088$ K, $X_{BaF_2} = 0.650$, respectively. The eutectic temperatures and the congruent melting point of $BaBO_2F$ agree very well with the measured data.

$Na_2B_2O_4$–2NaF system. The optimized parameters of the liquid phase derived from the measured data with $i = 2$ in Eq. [8] are listed in Table 3. The calculated phase diagram with the measured data is shown in Fig. 1. The calculated eutectic point is at $T = 1092$ K, $X_{2NaF} = 0.364$, which agrees very well with the measured data.

2NaF–BaF_2 system. The eutectic point measured by Bergman and Banashek (22) and the mixing enthalpy of liquid measured by Hong and Kleppa (24) were used in

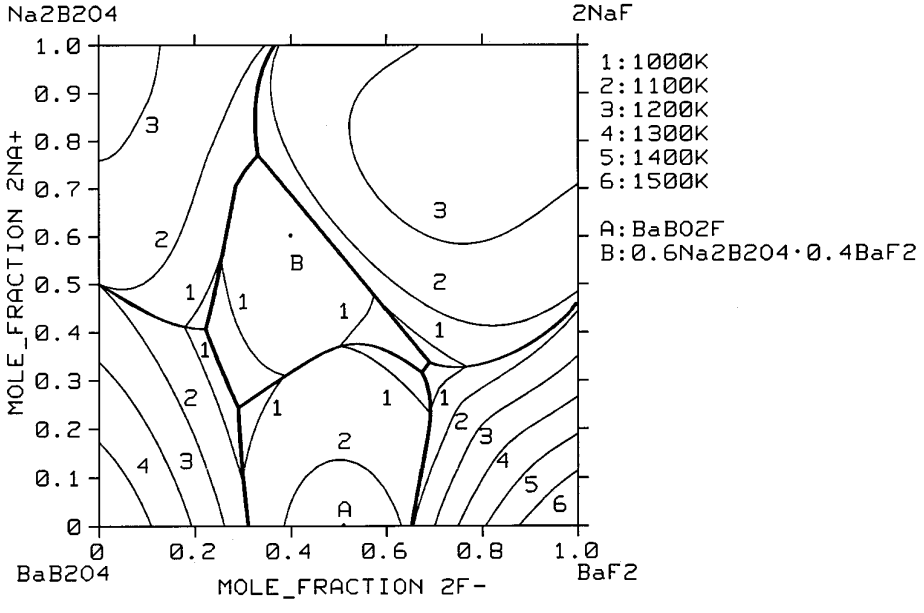

FIG. 8. Calculated phase diagram of the BaB_2O_4–BaF_2–2NaF–$Na_2B_2O_4$ reciprocal system.

TABLE 4
Compositions and Results of XRD Phase Analysis and DTA Measurement of Samples along the BaB_2O_4–$0.6Na_2B_2O_4 \cdot 0.4BaF_2$ Diagonal

No.	x_{2F^-}	x_{2Na^+}	XRD analysis	T°C (DTA measured)	T°C (calculated)
1	0.30	0.45	β-BaB_2O_4, B[a]	677, 744	687, 737
2	0.24	0.36	β-BaB_2O_4, B	687	687 (eutectic)
3	0.20	0.30	β-BaB_2O_4, B	661, 760	687, 761
4	0.16	0.24	β-BaB_2O_4, B	672, 826	687, 843
5	0.12	0.18	β-BaB_2O_4, B	690, 940	687, 923

[a] B represents $0.6Na_2B_2O_4 \cdot 0.4BaF_2$.

the optimization of the $2NaF$–BaF_2 binary system. The optimized parameters of the liquid phase are listed in Table 3. The calculated phase diagram is shown in Fig. 5. The calculated eutectic point is the same as the measured one (22). Figure 6 shows the calculated mixing enthalpy as well as the measured data. The calculated data agree with the measurement results (24).

$Na_2B_2O_4$–BaF_2 system. The optimized parameters of the liquid phase derived from the measured data in previous section with $i = 1$ in Eq. [8] are listed in Table 3. The Gibbs energy for solid $0.6Na_2B_2O_4 \cdot 0.4BaF_2$ was also optimized with $a_B + b_BT = -47848.74 + 26.04T$ J/mol in Eq. [4]. The calculated phase diagram and the measured data are shown in Fig. 2. The calculated eutectic points are at $T = 1024$ K, $X_{BaF_2} = 0.285$ and $T = 902$ K, $X_{BaF_2} = 0.675$, respectively. The eutectic temperatures and the congruent melting point of $0.6Na_2B_2O_4 \cdot 0.4BaF_2$ agree very well with the measured data.

In the range beyond $X_{BaF_2} = 0.80$ in all the systems containing BaF_2, the calculated temperature of the liquidus is obviously higher than the measured data. This disagreement is due to the use of the thermodynamic data of pure BaF_2 reported in Ref. (18). The melting point of BaF_2 reported in Ref. (18) (1640 K) is higher than that of our measured value (1586 K).

The optimization of all the binary systems was performed by using BINGSS and BINFKT programs (26). The final calculation of the binary phase diagrams was performed by using the Thermo-Calc program package (27).

4.4. Calculation of the BaB_2O_4–BaF_2–$2NaF$–$Na_2B_2O_4$ Phase Diagram

Calculation of the phase diagram of the BaB_2O_4–BaF_2–$2NaF$–$Na_2B_2O_4$ reciprocal system was performed with the Thermo-Calc program package (27). The thermodynamic model used in the calculation is described in Section 4.2. The thermodynamic parameters needed in the calculation are listed in Tables 2 and 3. The calculated phase diagram of the BaB_2O_4–BaF_2–$2NaF$–$Na_2B_2O_4$ reciprocal system is show in Figs. 7 and 8. In this reciprocal system, there are two kinds of cations, Ba^{2+} and Na^+, and two kinds of anions, $B_2O_4^{2-}$ and F^-. In Figs. 7 and 8, the abscisa represents the concentration of the anions and the ordinate represents the concentration of the cations. Figure 7 is the calculated liquid projection of this reciprocal system. E1 to E5 are the five eutectic points of this system. The eutectic temperatures and compositions of the five eutectic points are shown in Fig. 7. Figure 8 also shows several isotherms of liquidus surface from 1000–1500 K.

To verify the reliability of the calculated phase diagram, additional experiments were performed. To check whether the BaB_2O_4–$0.6Na_2B_2O_4 \cdot 0.4BaF_2$ diagonal is stable or not, five samples were prepared along this diagonal. Table 4 lists the compositions, the results of XRD phase analysis, and the DTA measurements of the samples. The results of XRD phase analysis show that all five samples contain two phases: β-BaB_2O_4 and $0.6Na_2B_2O_4 \cdot 0.4BaF_2$. This means that BaB_2O_4–$0.6Na_2B_2O_4 \cdot 0.4BaF_2$ is the stable diagonal. Compared with the DTA results, the calculated values are satisfactory by taking into consideration that these measured data are not included in the thermodynamic optimization.

The calculated phase diagram of the BaB_2O_4–BaF_2–$2NaF$–$Na_2B_2O_4$ reciprocal system indicates that this system may be a good flux system for growth of β-BaB_2O_4 single crystal, since the temperatures of eutectic points E4 (957 K) and E5 (948 K) are about 150 K lower than that of the BaB_2O_4–$Na_2B_2O_4$ system (1100 K), and the primary crystallization area of β-BaB_2O_4 is large.

5. CONCLUSIONS

The phase diagram of the BaB_2O_4–BaF_2–$2NaF$–$Na_2B_2O_4$ reciprocal system presented in this work is the result of an interactive use of conventional experimental techniques for phase diagram determination with thermodynamic computational optimization methods. The phase diagrams of the $Na_2B_2O_4$–$2NaF$ binary system and the $Na_2B_2O_4$–BaF_2 pseudo-binary system were measured and calculated. A new compound, $0.6Na_2B_2O_4 \cdot 0.4BaF_2$, was

synthesized. Based on the previous works and the works of other researchers, other sub-binary systems were also optimized and calculated. After being verified by additional experiments, the calculated phase diagram of the BaB_2O_4–BaF_2–2NaF–$Na_2B_2O_4$ reciprocal system based on the optimized results of the sub-binary systems may be considered to be reliable. This reciprocal system may be regarded as a good flux system for growth of large size β-BaB_2O_4 single crystals.

ACKNOWLEDGMENTS

The authors thank the National Natural Science Foundation of China for financial support, Professor H. L. Lukas for offering BINGSS and BINFKT programs, and Dr. Bo Sundman for the Thermo-Calc program package.

REFERENCES

1. C. T. Chen, B. H. Wu, A. D. Jiang, and G. M. You, *Sci. Sinica, B* **28,** 235 (1985).
2. E. M. Levin and H. F. Memurdie, *Nat. Bur. Stand. J. Res.* **42,** 131 (1949).
3. J. K. Liang, Y. L. Zhang and Q. Z. Huang, *Acta Chim. Sinica,* **40,** 994 (1982).
4. Q. Z. Huang, J. K. Liang, *Acta Phys. Sinica,* **30,** 559 (1981).
5. Q. Z. Huang, G. F. Wang and J. K. Lian, *Acta Phys. Sinica,* **33,** 75 (1984).
6. G. F. Wang, Q. Z. Huang and J. K. Liang, *Acta Chim. Sinica,* **42,** 503 (1984).
7. G. F. Wang and Q. Z. Huang, *Acta Phys. Sinica,* **34,** 562 (1985).
8. Q. Z. Huang, J. K. Liang and W. E. Gan, *Kexue Tongbao,* **31,** 610 (1986).
9. G. H. Rao, J. K. Liang, Z. Y. Qiao and Q. Z. Huang, *CALPHAD,* **13,** 169 (1989).
10. G. H. Rao, Z. Y. Qiao and J. K. Liang, *CALPHAD,* **13,** 177 (1989).
11. Q. Z. Huang and J. K. Liang, *J. Crystal Growth,* **97,** 720 (1989).
12. G. H. Rao, Z. Y. Qiao and J. K. Liang, *Acta Metall. Sinica,* **27,** B137 (1991).
13. G. H. Rao, Z. Y. Qiao and J. K. Liang, *Sci. China* (*Series A*), **36,** 1063 (1993).
14. L. Kaufman and H. Bernstein, ''Computer Calculation of Phase Diagrams.'' Academic Press, New York, 1970.
15. A. D. Pelton and M. Blander, *Metall. Trans. B,* **17,** 805 (1986).
16. T. I. Barry *et al*., *J. Phase Equil.,* **13,** 459 (1992).
17. Z. Y. Qiao *et al., Prog. Nat. Sci.* **5,** 463 (1995).
18. O. Knacke, O. Kubaschewski, and K. Hesselmann (Eds.), ''Thermochemical Properties of Inorganic Substances.'' 2nd ed. Springer-Verlag, Berlin/Heidelberg, 1991.
19. Q. Chen, Ph. D. Thesis, Central-south University of Technology, Changsha, 1995.
20. D. R. Stewart and G. E. Rindone, *J. Am. Ceram. Soc.,* **46,** 593 (1963).
21. M. Blander, ''Molten Salt Chemistry,'' p. 129. Interscience, New York, 1964.
22. A. G. Bergman and E. I. Banashek, *Izv. sektora. Fiz. Khim. Anal. Inst. Obshcheii. Neorg. Khim. Adad. Nauk. SSSR,* **22,** 196 (1953).
23. G. Grube, *Z. Electrochem.,* **33,** 481 (1927).
24. K. C. Hong and O. J. Kleppa, *J. Phys. Chem.,* **82,** 1596 (1978).
25. O. Redlich and A. Kister, *Ind. Eng. Chem.,* **40,** 345 (1948).
26. H. L. Lukas and S. G. Fries, *J. Phase Equil.,* **13,** 532 (1992).
27. B. Sundman, B. Jansson and J. O. Andersson, *CALPHAD,* **9,** 153 (1985).
28. G. A. Bukhalova and E. S. Yagub'yan, *Izv. Akad. Nauk. SSSR, Neorg. Mater.*, **3,** 1096 (1967).